Ex vivo and in vivo CRISPR/Cas9 screenings identify the roles of protein N-glycosylation in regulating T-cell activation and functions

Yu Hong[1, 2, 5], Xiaofang Si [1, 2, 3, 5], Wenjing Liu [1, 2, 3, 5], Xueying Mai[1, 2, 4, 5], Yu Zhang[1, 2, 3, 4 *]

[1]Institute for Cancer Research, Chinese Institutes for Medical Research, Beijing 100069，China

[2]National Institute of Biological Sciences, Beijing 102206, China;

[3]Chinese Academy of Medical Sciences & Peking Union Medical College, Beijing 100730, China;

[4]Capital Medical University, Beijing 100069, China.

[5]These authors contributed equally to this work.

*Correspondence should be addressed to Y. Z. (zhangyu@cimrbj.ac.cn ; zhangyu@nibs.ac.cn).

Abstract

Cytotoxic CD8$^+$ T-cells play central roles in tumor immunotherapy. Understanding mechanisms that regulate development, differentiation, and functions of cytotoxic CD8$^+$ T-cells leads to development of better immunotherapies. By combining primary T-cell culture and a syngeneic mouse tumor model with both genome-wide and custom CRISPR/Cas9 screenings, we systematically identified genes and pathways that regulate PD-1 expression and functions of CD8$^+$ T-cells. Among them, inactivation of a key enzyme in glycoconjugate biosynthesis, beta 1, 4-galatosyltransferase 1 (B4GALT1), leads to significantly enhanced T-cell receptor (TCR) activation and functions of CD8$^+$ T-cell. Interestingly, suppression of B4GALT1 enhances functions of TCR-T-cells, but has no effect on chimeric antigen receptor T (CAR-T) cells. We systematically identified the substrates of B4GALT1 CD8$^+$ T-cell surface by affinity purification and mass spectrometry analysis, which include protein components in both TCR and its co-receptor complexes. The galactosylation of TCR and CD8 leads to reduced interaction between TCR and CD8 that is essential for TCR activation. Artificially tethering TCR and CD8 by a TCR-CD8 fusion protein could bypass the regulation of B4GALT1 in CD8$^+$ T-cells. Finally, the expression levels of B4GALT1 normalized to tumor infiltrated CD8$^+$ T-cells in tumor microenvironment are significant and negatively associated with prognosis of human patients. Our results reveal the important roles of protein N-glycosylation in regulating functions of CD8$^+$ T-cells and prove that B4GALT1 is a potential target for tumor immunotherapy.

38 # Introduction

39 Cytotoxic CD8$^+$ T-cells play a central role in tumor immunotherapy. The presence and
40 activation status of CD8$^+$ T-cells in tumors are efficient biomarkers to predict prognostic
41 and therapeutic efficacy for patients receiving immunotherapy[1, 2]. Immune checkpoint
42 inhibitors (e.g., anti-PD-1, anti-PD-L1, and anti-CTLA4 antibodies) targeting the
43 reactivation of tumor-infiltrated cytotoxic CD8$^+$ T-cells have shown amazing clinical
44 benefits in treating various human tumors[3-7]. Chimeric antigen receptor T (CAR-T) and
45 T-cell receptor-engineered T (TCR-T) cells, which are exogenous cytotoxic CD8$^+$ T-
46 cells that are genetically engineered to directly target cancer cells, have demonstrated
47 promising clinical efficacy against some human tumors[8, 9]. Fully elucidating the
48 mechanisms regulating development, differentiation, and functions of cytotoxic CD8$^+$
49 T-cells paves ways for development of better tumor immunotherapies.

50 Expression of programmed cell death protein 1 (PD-1) can be induced in a wide variety
51 of immune cell types[10-12]. For example, TCR activation induces the expression of PD-
52 1 on T-cell surface. The interaction between PD-1 receptor and its ligand, PD-L1,
53 reduces TCR signals to suppress immune system. When tumors evade attacks from
54 the immune system, cancer cells upregulate their surface PD-L1 expression to prevent
55 attack by endogenous cytotoxic CD8$^+$ T-cells. Antibodies blocking the interaction
56 between PD-1 and PD-L1 have been proven to be effective in human tumor
57 immunotherapy and show high efficacy in many tumor types[4, 5]. Understanding how
58 immune cells regulate their PD-1 expression is one of the most important aspects of
59 tumor immunology research. Although a few regulators of PD-1 expression in cytotoxic
60 CD8$^+$ T-cells have been identified recently[13-17], an unbiased systematic screening is
61 still missing.

62 Here, by combining ex vivo primary memory CD8$^+$ T-cell culture and an in vivo
63 syngeneic mouse tumor model with genome-wide and custom CRISPR/Cas9
64 screenings, we systematically identified genes and pathways that regulate PD-1

expression and functions of $CD8^+$ T-cells. Among them, inactivation of a key enzyme in glycoconjugate biosynthesis, i.e., B4GALT1, enhances PD-1 expression, TCR activation, and functions of mouse $CD8^+$ T-cells both in vitro and in vivo. Similar roles of B4GALT1 were also observed in human $CD8^+$ T-cells. Mechanistic studies indicate that B4GALT1 regulates $CD8^+$ T-cell function via a TCR-dependent pathway through cell surface protein glycosylation. Systematic LC-MS analysis further identified that proteins in TCR-complex and its co-receptors are direct substrates of B4GALT1. Mechanistic studies indicate that B4GALT1 deficient T-cells showed stronger TCR-CD8 interaction and enhanced TCR activation than wild-type control, which can be bypassed by artificially tethering of TCR with CD8 when CD8β-CD3ε fusion protein was overexpressed. These results support a model that B4GALT1 modulates T-cell function by direct galactosylation of TCR and CD8 which prevents the interaction between them. Finally, the expression of B4GALT1 showed a significant negative correlation with prognosis of human cancer patients when normalized to tumor infiltrated $CD8^+$ T-cells. Taken all together, the results reveal the important roles of protein N-glycosylation in regulating functions of $CD8^+$ T-cells and prove that B4GALT1 is a potential target for tumor immunotherapy.

82 ## Results

83 Ex vivo and in vivo CRISPR/Cas9 screenings identify genes and pathways that
84 regulate PD-1 expression and functions of CD8$^+$ T-cells

85 We set up an ex vivo genome-wide CRISPR/Cas9 screening system to identify genes
86 and pathways that regulate PD-1 expression in mouse primary CD8$^+$ T-cells (Fig. 1a).
87 In brief, splenic CD8$^+$ T-cells from Cas9-EGFP/OT-I mice were infected with a retroviral
88 whole-genome guide RNA (gRNA) library following ovalbumin (Ova) peptide
89 stimulation. After puromycin selection, the memory CD8$^+$ T-cells were re-stimulated by
90 co-culturing with B16F10-OVA cells. The highest and lowest 5% PD-1$^+$ cells were
91 isolated by fluorescence-activated cell sorting (FACS) and defined as PD-1^{high} and PD-
92 1^{low} populations, respectively. The distributions of individual gRNAs in the whole-
93 genome library in those subpopulations, as well as in input cells, were revealed by
94 next-generation sequencing. As shown in Fig. 1b, *Pdcd1* and previously identified PD-
95 1 regulators, such as *Satb1*[14] and *Fut8*[15], were successfully identified as positive
96 controls. We could verify most of the top candidates individually by FACS and RT-
97 qPCR assays (Fig. 1c). Gene set enrichment analysis (GSEA) identified several KEGG
98 (Kyoto Encyclopedia of Genes and Genomes) pathways significantly involved in
99 regulation of PD-1 expression in CD8$^+$ T-cells (Fig. 1d). As expected, genes that are
100 known to be involved in the T-cell receptor (TCR) activation pathway such as *Cd3d*,
101 *Zap70*, and *Lat* were among the top ones identified. Interestingly, genes involved in
102 protein export pathway (such as *Srp14*, *Srp68*, *Sec16A*) and in aminoacyl tRNA
103 biosynthesis (such as *Mars*, *Hars2*, *Eprs*) were significantly increased in PD-1^{low}
104 populations. In addition, we also identified and verified genes required for N-glycan
105 biosynthesis, including *B4galt1*, *Mgat2*, and *Dpm3*, which could negatively regulate the
106 expression of PD-1 (Fig. S1a-c).

107 To verify these candidate genes in a high-throughput manner, we synthesized a
108 custom gRNA library containing 4,617 gRNAs targeting the top candidate genes

109 obtained from whole-genome screenings and 105 intergenic control gRNAs. The
110 gRNA library-infected Cas9-EGFP/OT-I memory CD8$^+$ T-cells were restimulated by
111 co-culture and PD-1 regulators were enriched using the same strategy as whole-
112 genome screening (fig. 1a). As shown in fig. 2b, most of the significant PD-1 regulators
113 in the top list of genome-wide screening could also be enriched in the custom small
114 library screening, which indicates the reliability of our ex vivo screenings. To test
115 potential functions of these candidate genes in the context of tumor microenvironment,
116 custom gRNA-library-infected Cas9-EGFP/OT-I memory CD8$^+$ T-cells were
117 transplanted into wild-type (WT) C57BL/6J mice inoculated subcutaneously (s.c.) with
118 B16F10-OVA tumors to screen for genes regulating CD8$^+$ T-cell functions in vivo. After
119 7 days, tumor-infiltrated CD8$^+$ T-cells were collected for gRNA sequencing (Fig. 2a).
120 We successfully identified several positive control genes[18-21] such as *Socs1*,
121 *Regnase-1 (Zc3h12a)*, *Rc3h1*, and *Cd36*, indicating our in-vivo screening system
122 worked robustly (Fig. 2c). Interestingly, inactivating *B4galt1*, which encodes beta-1,4-
123 galactosyltransferase 1, showed significant phenotypes in both ex vivo and in vivo
124 screenings.

125

126 <u>B4GALT1 suppression in CD8$^+$ T-cells activates TCR signaling and enhances T-cell</u>
127 <u>functions both in vitro and in vivo</u>

128 B4GALT1 is one of the seven beta-1,4-galactosyltransferases that transfer galactose
129 in a beta 1-4 linkage to similar acceptor sugars, including N-acetylglucosamine
130 (GlcNAc), glucose (Glc), and xylose (Xyl). More specifically, B4GALT1 uses UDP-
131 galactose and N-acetylglucosamine for the production of galactose beta-1,4-N-
132 acetylglucosamine[22]. In addition to glycoconjugate biosynthesis, B4GALT1 can also
133 form a heterodimer with a-lactalbumin (LALBA) as lactose synthetase in lactating
134 tissues. Although B4GALT1 is expressed ubiquitously, its roles in regulating interaction
135 and adhesion of immune cells have been suggested[23-28].

136 Infection of Cas9-EGFP/OT-I $CD8^+$ T-cells with different gRNAs targeting B4galt1
137 resulted in significantly increased surface PD-1 expression and PD-1 mRNA levels
138 both before and after co-culture with B16F10-OVA cells (Fig. 3a and Fig. S1c). Such
139 phenotypes could be rescued by overexpression of either a short or long isoform of
140 mouse *B4galt1* cDNA (Fig. 3b), suggesting that biosynthetic function, but not ligand-
141 induced signal transduction, of B4GALT1[22] is responsible for suppression of PD-1
142 expression. In addition, *B4galt1* deficient OT-I T-cells showed enhanced expression of
143 T-cell activation and cytotoxic markers such as IFNγ and TNFα (Fig. 3c), as well as in
144 vitro targeted cell killing activity when co-cultured with target cells, B16F10-OVA (Fig.
145 3d). To verify whether B4GALT1 has similar functions in human T-cells, we infected
146 primary human $CD8^+$ T-cells with NY-ESO-1 TCR constructs containing shRNA
147 expression cassettes targeting human B4GALT1[29] (Fig. 3e). As shown in Fig 3f,
148 comparing with control, knockdown of human B4GALT1 enhanced targeted killing of
149 human A375 cells in vitro. Increased secretion levels of IFNγ and TNFα have been
150 observed after knockdown of B4GALT1 (Fig. 3g). Surprisingly, knockout of B4GATL1
151 could not affect hCD19-CAR mediated in vitro killing of Nalm6 cells (Fig. S2a). When
152 stimulate with only anti-CD3/28 antibodies in the absence of target cells, B4GALT1
153 knockout OT-I cells also did not show significantly enhanced expression of IFNγ and
154 TNFα, comparing with controls (Fig. S3a). These results indicate that B4GALT1 may
155 enhance T-cell functions via a TCR- and target-cell dependent pathway.

156 To dissect mechanisms by that B4GALT1 regulates T-cell functions, we sorted OT-I T-
157 cells after co-culture with target cells for genome-wide transcriptional analysis. Whole-
158 genome RNA sequencing analysis confirmed the enhanced TCR activation in *B4galt1*
159 knockout $CD8^+$ T-cells (Fig. 3h-j). GSEA of DEGs (differentially expressed genes)
160 between control and *B4galt1* gRNA-infected $CD8^+$ T-cells revealed that TCR signaling
161 pathway was at the top of significantly altered pathways (Fig. 3j).

162 When transplanted into wild-type mice with B16F10-OVA cells inoculated
163 subcutaneously, *B4galt1* gRNA-infected OT-I T-cells showed significantly higher tumor

164 killing activity than control gRNA-infected cells (Fig. 4a-c). Analysis of tumor-infiltrated
165 lymphocytes (TILs) demonstrated more infiltrated OT-I T-cells in tumors when *B4galt1*
166 gRNA was infected (Fig. 4d). Mechanistically, B16F10-OVA tumors had similar
167 numbers of infiltrated *B4galt1* gRNA-infected OT-I T-cells as control gRNA-infected
168 cells 24 hours after intravenous injection (Fig. S4a), suggesting that B4GALT1 has no
169 significant effect on initial tumor infiltration of OT-I T-cells. On the other hand, CFSE
170 (carboxyfluorescein succinimidyl ester) analysis at a later time point (6 days after
171 infusion) showed increased OT-I T-cell proliferation within tumors when B4GALT1 was
172 inactivated (Fig. S4b). Altogether, these results suggest that inhibition of N-
173 galactosylation could enhance functions of $CD8^+$ T-cells both in vitro and in vivo, and
174 that B4GALT1 could be a potential target to modulate activity of T-cells.

175

176 <u>Systematically identification of direct substrates of B4GALT1 on T-cell surface</u>

177 To dissect the molecular mechanism by which B4GALT1 regulates T-cell activation,
178 we analyzed N-glycome on OT-I T-cell surface by FACS staining (Fig. S5a). Biotin-
179 labeled *Erythrina cristagalli* lectin (ECL) and succinyl-wheat germ agglutinin (sWGA)
180 were used to profile surface expression of terminal βGal and βGlcNAc, respectively.
181 *B4galt1* knockout OT-I T-cells showed slightly but significantly decreased ECL
182 staining and significantly increased sWGA staining, comparing with WT control T-
183 cells (Fig. S5b-c). FACS staining with biotin-labeled recombinant Galectin-1 (Gal-1)
184 showed a more dramatic difference between control and *B4galt1* knockout OT-I T-
185 cells (Fig. S5d).

186 To identify potential substrates of B4GALT1 on $CD8^+$ T-cell surface, we used a
187 recombinant Gal-1 affinity column and lactose elution to purify N-glycosylated
188 proteins from whole membrane-protein extracts of OT-I $CD8^+$ T-cells (Fig. 5a). LC-
189 MS analysis of proteins that were significantly different between control and *B4galt1*
190 knockout OT-I T-cells revealed that both TCRα/β (OT-I) and CD8α/β were among

191 the top list (Fig. 5b). KEGG analysis also showed a significant enrichment of TCR
192 signaling pathway (Fig. 5c). We could verify reduced Gal-1 pull-down for CD8β and
193 most of other hits in *B4galt1* knockout T-cells by western blotting with commercially
194 available antibodies (Fig. 5d). Interestingly, migration of CD8β in SDS-PAGE was
195 significantly different between control and *B4galt1* knockout T-cell extracts,
196 suggesting that CD8β is a direct substrate of B4GALT1 (Fig. 5d). Indeed, treating
197 whole membrane-protein extracts with PNGase F to remove all N-linked
198 glycosylation on proteins omitted the migration difference of CD8β and most of other
199 hits we identified (Fig. 5e).

200 It has been suggested that interaction between TCR and CD8 plays an important
201 role for TCR activation[30, 31]. We hypothesized that aberrant galactosylation of TCR
202 and CD8 might directly affect their interaction. As shown in Fig. 5f, FRET signals of
203 TCR-CD8 increased significantly in B4GALT1 deficient T-cells, comparing with
204 control wild-type cells. To confirm whether reduced TCR-CD8 interaction is the
205 major cause of TCR activation phenotype in B4GALT1 knockout $CD8^+$ T-cells, we
206 generated a construct which fused the CD8β ectodomain (ECD) with CD3ε (Fig.5g).
207 Overexpression of such CD8β-CD3ε fusion led to enhanced in vitro killing activities
208 in wild-type $CD8^+$ T-cells. On the other hand, the enhanced T-cell killing activities by
209 B4GALT1 knockout was significantly diminished when fusion construct was
210 overexpressed in B4GALT1 knockout $CD8^+$ T-cells (Fig.5h-i). Taken together, these
211 results support a model that B4GALT1 directly regulates galactosylation of TCR
212 complex and co-receptors to regulate TCR-CD8 interaction, which is essential for
213 TCR activation and functions of T-cells.

214

215 <u>The expression levels of B4GALT1 and tumor infiltrated $CD8^+$ T-cells in tumor</u>
216 <u>microenvironment are associated with prognosis of human patients</u>

217 To investigate potential clinical relevance of B4GALT1 in human tumor patients, we
218 analyzed cancer samples in The Cancer Genome Atlas (TCGA)[32]. While expression
219 levels of B4GALT1 are not linked to an overall survival benefit using data of all TCGA
220 collected primary cancer samples, after normalized to expression level of CD8A,
221 Kaplan-Meier curve showed a significantly better survival duration in patients with low
222 expression of B4GALT1 (Fig. S6a-b)[33]. In Adrenocortical carcinoma (ACC), Acute
223 Myeloid Leukemia (LAML), Lung adenocarcinoma (LUAD), and Rectum
224 adenocarcinoma (READ) data sets, for patients with higher expression of CD8A, low
225 B4GALT1 expression level is significantly associated to better overall survival,
226 comparing with patients with lower expression of CD8A (Fig. 6a and Fig. S6c). On the
227 contrary, in patients with lower expression of B4GALT1, high CD8A expression level
228 is significantly associated to better overall survival, comparing with patients with higher
229 expression of B4GALT1 (Fig. 6b and Fig. S6c). Collectively, these data suggested
230 expression of B4GALT1 in tumor microenvironment and presence of tumor infiltrated
231 $CD8^+$ T-cells are jointly associated with prognosis of cancer patients.

232

233 ## Discussion

234 Cytotoxic CD8$^+$ T-cells, which directly kill tumor cells, are key effector cells within tumor
235 microenvironment[34, 35]. Following TCR activation by MHC-peptide complexes, PD-1
236 expression in T-cells is significantly upregulated[36, 37]. Cytokines, such as IL-2, IL-7,
237 and interferons secreted by T-cells, can also induce high PD-1 expression[38]. Beyond
238 its role as one of the markers for TCR activation, PD1 suppresses further T-cell
239 activation after binds to its ligand PD-L1, thereby preventing excessive immune
240 responses[39]. Therapeutically targeting PD-1 molecules on immune cells, especially
241 cytotoxic CD8$^+$ T-cells, is one of the most successful strategies to treat tumors[5].
242 Understanding the mechanisms that regulate PD-1 expression on cytotoxic CD8$^+$ T-
243 cells presents important clues to optimize current tumor immunotherapy strategies,
244 including CAR-T/TCR-T and immune checkpoint inhibitors, especially anti-PD-1 and
245 anti-PD-L1 blocking antibodies.

246 By genome-wide CRISPR/Cas9 screenings, we systematically identified genes and
247 pathways regulating PD-1 expression in primary CD8$^+$ T-cells. The results that *Pdcd1*
248 gene and some previously reported regulators of PD-1, such as *Satb1* and *Fut8*, were
249 successfully identified, demonstrate the effectiveness of this screening system.
250 Interestingly, genes in N-glycan biosynthesis are significantly enriched to negatively
251 regulate PD-1 expression in CD8$^+$ T-cells. Inhibition of B4GALT1 could activate
252 expression of PD-1 and functions of CD8$^+$ T-cells both in vitro and in vivo.
253 Mechanistically, B4GALT1 modulates galactosylation of proteins on CD8$^+$ T-cell
254 surface, including proteins in TCR complex and its co-receptors. The decreased
255 galactosylation of TCR complex and CD8 enhances the TCR-CD8 interaction, which
256 is the major downstream mechanism that B4GALT1 regulates TCR activation. Our
257 results not only demonstrate the important roles of protein N-glycosylation in regulating
258 functions of CD8$^+$ T-cells but also prove that B4GALT1 is an effective target for tumor
259 immunotherapy. In particular, previous studies have demonstrated the roles of

260 B4GALT1 in cancer cells such as in LUAD and CRC[26-28]. Our study suggests that
261 inhibition of B4GALT1 in both cancer cells and $CD8^+$ T-cells may synergistically
262 suppress tumor growth.

263 Based on results from individual studies of specific glycosidases and
264 glycosyltransferases, N-linked glycosylation of T-cell surface proteins have been
265 proposed to regulate T-cell development, activation, and functions[40]. Here, we
266 identified roles of N-glycome synthesis in regulating PD1 expression of $CD8^+$ T-cells
267 by unbiased genome-wide screenings. To further investigate mechanisms, we
268 systematically characterized substrates of B4GALT1 on $CD8^+$ T-cell surface,
269 suggesting the model that B4GALT1 regulates TCR activation by directly modulate N-
270 glycosylation of components of TCR and its co-receptor complexes. In addition,
271 several interesting observations also provides mechanistic insights supporting our
272 hypothesis. Knockout of B4GALT1 only significantly affect activation of exogenous and
273 exogenous TCR (OT-I and NY-ESO-1, respectively) but not CAR (hCD19-CAR) in
274 $CD8^+$ T-cells. Similarly, knockout of CD8a shows different effect on TCR and CAR
275 activation (data not shown). Moreover, different from results obtained after co-culture
276 with target cells, when B4GALT1 knockout $CD8^+$ T-cells were stimulated by anti-
277 CD3/28 only, they did not show significantly enhanced activation. Further studies are
278 necessary to clarify whether B4GALT1 mediated N-galactosylation modifications
279 directly or indirectly affect functions of its substrates and how target cancer cells
280 contribute to activation of $CD8^+$ T-cells in a B4GALT1-dependent manor.

281 Adoptive T-cell therapy has been actively implicated for treatment of cancer and
282 chronic infections[41, 42]. While CAR-T and TCR-T therapies demonstrated promising
283 effect in controlling hematological malignancies, their applications in solid tumors
284 remains challenging[43, 44]. How to enhance activities of in vitro expanded T-cells is also
285 a major barrier for tumor-infiltrating lymphocyte (TIL) therapy[45]. Our in vitro and in vivo
286 results strongly support that B4GALT1 is a potential target to enhance the efficacy of
287 adoptive T-cell therapy.

288 In summary, our study utilized unbiased genome-wide and custom small library
289 screenings to identify PD-1 regulators in $CD8^+$ T-cells, and discovered a fundamental
290 role for a gene involved in N-glycan biosynthesis---B4GALT1, which can enhance T-
291 cell activation and functions both in vitro and in vivo. Our findings highlight the power
292 of protein N-glycosylation in regulating functions of $CD8^+$ T-cells and suggest that
293 B4GALT1 is a potential target for tumor immunotherapy. It will provide a new
294 perspective and direction for the research of T-cell regulators to enhance the efficacy
295 of tumor immunotherapy.

Declarations

Ethics approval and consent to participate

All animal experiments were conducted following the Ministry of Health national guidelines for housing and care of laboratory animals and performed in accordance with institutional regulations after review and approval by the Institutional Animal Care and Use Committee at the National Institute of Biological Sciences and Chinese Institutes for Medical Research. The assigned approval/accreditation number: AEEI-2023-223.

This manuscript does not report on or involve the use of any human data or tissue.

Consent for publication

This manuscript does not contain data from any individual person.

Availability of data and materials

The raw sequence data reported in current study have been deposited in the Genome Sequence Archive in BIG Data Center, Beijing Institute of Genomics (BIG), Chinese Academy of Sciences, under accession numbers PRJCA010494 that can be accessed at https://ngdc.cncb.ac.cn/search/?dbId=&q=PRJCA010494.

Other materials used during the current study are available from the corresponding author on reasonable request.

Competing interests

Part of this research has been submitted for a patent.

Funding

The research in Y.Z. lab is supported by grants from National Key R&D Program of China (2021YFA1101002), National Natural Science Foundation of China (81773304,

81572795), the “Hundred, Thousand and Ten Thousand Talent Project” by Beijing municipal government (2019A39).

Authors' contributions

Y.H. and Y.Z. conceived the study. Y.H., X.S., W.L., X.M. performed experiments and analyzed data. Y.Z. analyzed data and wrote the manuscript with support from all authors.

Acknowledgments

We thank members of Y.Z. lab for helpful discussion and support. We thank Dr. Songbiao Zhu at Proteomics Center (CIMR) for assistance with LC-MS analysis. We thank the municipal government of Beijing and the Ministry of Science and Technology of China for funds allocated to CIMR and NIBS.

330 **Figure legends:**

331 **Figure 1. Ex vivo CRISPR/Cas9 screenings identify genes and pathways that**
332 **regulate PD-1 expression of CD8$^+$ T-cells.**

333 a. Schematic view of ex vivo CRISPR/Cas9 screening in mouse primary CD8$^+$ T-cells.
334 b. Volcano plot showing results of ex vivo CRISPR/Cas9 genome-wide screenings.
335 The p-values were calculated using the α-robust rank aggregation (α-RRA)
336 algorithm in MAGeCK.
337 c. Verification of candidate genes by individual gRNAs. The relative expression levels
338 of surface PD-1 protein and PD-1 mRNA were measured by FACS as mean
339 fluorescent intensity (MFI) and RT-qPCR, respectively.
340 d. GSEA of significantly enriched KEGG pathways in genome-wide screening. The
341 enrichment score (ES) and statistical significance were calculated using the
342 clusterProfiler (version 3.12.0) R package.

343 **Figure 2. In vivo CRISPR/Cas9 screenings with a custom gRNA library identify**
344 **genes that regulate functions of CD8$^+$ T-cells in tumor microenvironment.**

345 a. Schematic view of in vivo CRISPR/Cas9 screening in mouse primary CD8$^+$ T-cells.
346 b. Volcano plot showing results of ex vivo CRISPR/Cas9 screening. The p-values
347 were calculated using the α-RRA algorithm in MAGeCK.
348 c. Volcano plot showing results of in vivo CRISPR/Cas9 screenings. The p-values
349 were calculated using the α-RRA algorithm in MAGeCK.

350 **Figure 3. B4GALT1 suppression in CD8$^+$ T-cells activates TCR signaling and**
351 **enhances T-cell functions.**

352 a. CRISPR/Cas9 knockout of *B4galt1* (sgB4galt1) in CD8$^+$ T-cells increases
353 expression of PD-1 before and after co-culture with B16F10-OVA cells. The MFIs
354 of PD-1 were measured by FACS. The relative mRNA levels of PD-1 were
355 measured by quantitative RT-qPCR. The p-values were calculated using a two-
356 tailed Student's t-test.

b. The effect of *B4galt1* knockout on PD-1 surface expression could be rescued by overexpression of either long- or short-isoform B4galt1. The p-values were calculated using a two-tailed Student's t-test.

c. CRISPR/Cas9 knockout of *B4galt1* in $CD8^+$ T-cells increases expression of TNFα and IFNγ after co-culture with B16F10-OVA cells. The relative mRNA levels were measured by quantitative RT-qPCR. The secreted TNFα and IFNγ in medium were measured by ELISA. The p-values were calculated using a two-tailed Student's t-test.

d. CRISPR/Cas9 knockout of *B4galt1* in OT-I $CD8^+$ T-cells increases in vitro specific killing activities on B16F10-OVA cells. The p-values were calculated using a two-tailed Student's t-test.

e. Schematic view of B4GALT1 knockdown in human NY-ESO-1 TCR-T-cells.

f. Knockdown of B4GALT1 in human NY-ESO-1 TCR-T-cells by shRNA increases in vitro killing activities on A375 cells. The p-values were calculated using a two-tailed Student's t-test.

g. Knockdown of B4GALT1 in human NY-ESO-1 TCR-T-cells increases expression of TNFα and IFNγ after co-culture with A375 cells. The secreted TNFα and IFNγ in medium were measured by ELISA. The p-values were calculated using a two-tailed Student's t-test.

h. Heatmap demonstrating differentially expressed genes (DEGs) between B4galt1 knockout and control mouse OT-I $CD8^+$ T-cells after co-culture. The genes in TCR signaling pathway are labeled on the left side.

i. Volcano plot showing upregulated and downregulated genes (p-value<0.01) in B4galt1 knockout mouse OT-I $CD8^+$ T-cells after co-culture. The genes in TCR signaling pathway are labeled with dark blue and dark red. Top genes and some genes in TCR signaling pathway are annotated. The p-value was calculated using the Wald test, and p.adjust was calculated using Benjamini-Hochberg with the R package DESeq2 (version 1.22.2).

j. Bar graph showing KEGG pathways significantly changed in *B4galt1* knockout

386 mouse OT-I $CD8^+$ T-cells after co-culture. The p-value was calculated using the
387 clusterProfiler (version 3.12.0) R package.

388 Data are shown as the mean ± SEM. *P < 0.05; **P < 0.01; ***P < 0.001.

389 **Figure 4. Knockout of *B4galt1* in $CD8^+$ T-cells enhances T-cell-mediated tumor**
390 **immunotherapy.**

391 a. Schematic view of *B4galt1* functional test in tumor microenvironment.
392 b. CRISPR/Cas9 knockout of B4galt1 in OT-I T-cells enhances growth control of
393 B16F10-OVA tumors in vivo. The p-value was calculated using two-way ANOVA.
394 c. Compared with control OT-I T-cells, the tumors were significantly smaller when
395 B4galt1 knockout OT-I T-cells were transplanted. The p-value was calculated using
396 a two-tailed Student's t-test.
397 d. CRISPR/Cas9 knockout of B4galt1 increases numbers of OT-I T-cells in B16F10-
398 OVA tumors. The p-value was calculated using a two-tailed Student's t-test.

399 Data are shown as the mean ± SEM. *P < 0.05; **P < 0.01.

400 **Figure 5. Systematic identification of direct substrates of B4GALT1 on T-cell**
401 **surface.**

402 a. Schematic view of recombinant Gal-1 pulldown and LC-MS experiments.
403 b. Volcano plot showing identified Gal-1 binding proteins in control and B4galt1
404 knockout OT-I cells. Proteins among the top list were annotated and labeled with
405 red (decreased in *B4galt1* knockout) and green (increased in *B4galt1* knockout).
406 Proteins in TCR signaling pathway are underlined. The p-values were calculated
407 using Limma in DEqMS (V1.8.0).
408 c. Bar graph showing KEGG pathways significantly changed in *B4galt1* knockout OT-
409 I T-cells. The p-value was calculated using the clusterProfiler (version 3.12.0) R
410 package.
411 d. Western blot verification of pulldown hits in top list.
412 e. N-glycome analysis with PNGase F suggests that CD8β is a direct substrate of

413 B4GALT1.

414 f. Compared with wild-type control, B4GALT1 knockout OT-1 T-cells showed stronger

415 TCR-CD8 FRET signals.

416 g. Schematic view of CD8β-CD3ε fusion construct.

417 h. Overexpression of CD8β-CD3ε complex bypassed the effect of B4GALT1 on T-

418 cell in vitro killing activities.

419 All of the p-values were calculated by a two-tailed Student's t test. Data are shown as

420 the mean ± SEM. *P < 0.05; **P < 0.01; ***P < 0.001; NS, not significant.

421 **Figure 6. The expression levels of B4GALT1 and tumor infiltrated CD8$^+$ T-cells in**

422 **tumor microenvironment are associated with prognosis of human patients.**

423 a. The association between B4GALT1 expression levels and overall survival for

424 patients with different CD8A levels in TCGA-ACC, -LAML, -LUAD, and -READ

425 cohorts.

426 b. The association between CD8A expression levels and overall survival for patients

427 with different B4GALT1 levels in TCGA-ACC, -LAML, -LUAD, and -READ cohorts.

428 The p-values for all survival curves were calculated using two-sided Log-rank test.

429 **Methods**

430 **Cell lines**

431 HEK293T cell line was purchased from ATCC. B16F10 cell line was provided by
432 laboratory of Dr. Ting Chen (National Institute of Biological Sciences, Beijing). Nalm6
433 cell line was provided by laboratory of Dr. Zhaoqing Ba (National Institute of Biological
434 Sciences, Beijing). A375 cell line was provided by laboratory of Dr. Feng Shao
435 (National Institute of Biological Sciences, Beijing). B16F10-OVA cell line was
436 constructed by infecting B16F10 cells with lentivirus encoding chicken ovalbumin.

437 B4galt1 rescue vectors were constructed based on pMSCV-U6 sgB4galt1-PGK-puro-
438 2A-BFP vector. Long isoform (UniProt, P15535-1) and short isoform (UniProt, P15535-
439 2) were amplified from cDNA of mouse T-cells, and used to replace the BFP fragment
440 by seamless cloning kit (Biomed, CL116).

441 CD8β-CD3ε fusion vector was constructed by fusing CD8β ectodomain (ECD) and its
442 signal peptide with, a linker region, and the full-length of CD3ε, based on pMSCV-U6
443 sgB4galt1/empty-PGK-puro-2A-BFP vector mentioned above.

444 HEK293T, B16F10 and A375 cells were cultured in DMEM (Gibco C11965500BT)
445 supplemented with 10% fetal bovine serum (FBS), 2 mmol L-glutamine, 100 μg/ml
446 penicillin, and 100 U/ml streptomycin (all purchased from Gibco). Nalm6 cells were
447 maintained in RPMI-1640 (HyClone) medium supplemented with 15% FBS, 100 μg/ml
448 penicillin, 100 U/ml streptomycin, 10 mM HEPES, 0.1 mM 2-mercaptoethanol, 2 mM
449 L-glutamine and 1xMEM nonessential amino acids.

450 **Retrovirus and lentivirus preparation**

451 Retrovirus was packaged by co-transfecting HEK293T cells with MSCV vector and
452 pCL-Eco. 48 hours post-transfection, supernatant was collected and filtered through a
453 0.45 μm filter to remove cell debris. Virus was then concentrated by centrifugation in
454 Beckman Optima L-100XP (SW32Ti) at 25,000 rpm (107,000 g) for 2.5 hours at 4 °C

455 and resuspended in RPMI-1640 basic medium.

456 Lentivirus was packaged by co-transfecting HEK293T cells with lentiviral vector,
457 psPAX2, and pMD2.G. 48 hours post-transfection, supernatant was collected and
458 filtered through a 0.45 μm filter to remove cell debris. Virus was used for infection
459 directly or concentrated by centrifugation at 25,000 rpm (107,000 g) for 2.5 hours at
460 4 °C and resuspended in PBS.

461 To produce lentivirus for human $CD8^+$ T-cell infection, HEK293T cells were seeded in
462 Opti-MEM I Reduced Serum Medium (Gibco, 31985-070) supplemented with 5% FBS,
463 1 mM sodium pyruvate (Gibco, 11360-070), and 1xMEM nonessential amino acids
464 (Gibco, 11140-050) the day before transfection. 6 hours post-transfection, the
465 transfection medium was replaced with fresh medium supplemented with 1x ViralBoost
466 (Alstem Bio, VB100). Lentivirus was collected and filtered through a 0.45 μm filter 24
467 hours and 48 hours after transfection separately, followed by addition of Lenti-X-
468 Concentrator (Takara, 631232). Lentivirus was concentrated following manufacturer's
469 instructions and resuspended in X-VIVO 15 medium (Lonza, 04-418Q) in 1% of the
470 original volume.

471 **Animals**

472 Female C57BL/6J mice were purchased from Beijing Vital River Laboratory Animal
473 Technology Co., Ltd. OT-I mice were provided by laboratory of Dr. Hai Qi (Tsinghua
474 University). Cas9-EGFP/OT-I mice were generated by breeding OT-I and Cas9-EGFP
475 knock-in mice [46] at animal facility of the National Institute of Biological Sciences,
476 Beijing. Six- to eight-week-old mice were used at the start of experiments. Animals
477 were housed under specific pathogen-free conditions in individually ventilated cages
478 in a controlled 12-h day-night cycle with standard food and water provided ad libitum.
479 All animal experiments were conducted following the Ministry of Health national
480 guidelines for housing and care of laboratory animals and performed in accordance
481 with institutional regulations after review and approval by the Institutional Animal Care

482 and Use Committee at the National Institute of Biological Sciences.

483 **Retroviral whole-genome CRISPR/Cas9 gRNA library construction**

484 A whole-genome CRISPR knockout gRNA library (1000000096) was purchased from
485 Addgene. The gRNA regions were PCR amplified with primer pair F:5'-
486 GGCTTTATATATCTTGTGGAAAGGACGAAACACCG-3' and R:5'-
487 CTAGCCTTATTTTAACTTGCTATTTCTAGCTCTAAAAC-3', and then transferred into
488 MSCV-gRNA-PGK-PURO-2A-BFP vector by Gibson reaction.

489 **Retroviral small custom gRNA library construction**

490 A total of 1,398 genes were selected according to whole-genome knockout screening
491 results. On average, three gRNAs were selected from the initial library for each gene
492 according to gRNA performance (Supplementary Table 3). A total of 105 intergenic
493 control gRNAs were also added. Oligonucleotides containing the guide sequence were
494 synthesized (Custom Array), PCR-amplified, and cloned into MSCV-gRNA-PGK-
495 PURO-2A-BFP vector via Gibson reaction.

496 **Ex vivo T memory cell culture, infection, and adoptive transfer**

497 On Day 0, splenocytes were prepared from 6- to 8-week-old Cas9-EGFP/OT-I female
498 mice and cultured with IL2 (10 ng/ml) and SIINFEKL peptide (10 ng/ml) in complete
499 RPMI media (RPMI 1640, 10% FBS, 20 mM HEPES, 1 mM sodium pyruvate, 0.05 mM
500 2-mercaptoethanol, 2 mM L-glutamine, 100 U/ml streptomycin, and 100 μg/ml penicillin)
501 at a density of $1X10^6$ cells/ml for 24 hours. On day 1, activated Cas9-EGFP/OT-I T-
502 cells were enriched by Percoll isolation as previously described[47] and spin-infected
503 (2,000 g, 30 °C, 1 hour, with minimum acceleration and no brake) with retrovirus
504 supplemented with polybrene (8 μg/ml) in 24-well-plate. After spin-infection, the plate
505 was placed into a CO_2 incubator at 37 °C for 5 hours and cultured with IL2 (2 ng/ml),
506 IL7 (2.5 ng/ml), and IL15 (10 ng/ml) in complete RPMI media at a density of $3x10^5$
507 cells/ml. Two days after infection (Day 3), cells were selected by 3 μg/ml puromycin in
508 the presence of IL2/IL7/IL15 for another 4 days. On day 7, cells were used for co-

509 culture experiments or adoptive transfer.

510 **Human T-cell isolation, culture and transduction**

511 Human peripheral blood mononuclear cells (PBMC) were acquired from healthy
512 donors. $CD8^+$ T-cells were isolated using EasySep negative selection kit (STEMCELL,
513 Cat#17953), and stimulated with anti-CD3/CD28 Dynabeads (Thermo Fisher Scientific,
514 Cat#40203D). T-cells were cultured in X-VIVO medium with 10% FBS, 2 mmol L-
515 glutamine, 100 μg/ml penicillin, 100 U/ml streptomycin, and human IL2 (500 IU/ml). 48
516 hours after activation, T-cells were transduced in a lentivirus-coated plate, centrifuged
517 at 1,200 g for 90 minutes at 37℃. Lentivirus transduction was repeated once 24 hours
518 later. Positive transduced cells were sorted 3 days later. During T-cell expansion, the
519 cells were maintained at a concentration of 3 x 10^5 cells/ml.

520 **Anti-CD19-CAR and NY-ESO-1 specific TCR-T-cell generation**

521 pMSCV-CD19 scFv (FMC63)-IRES-RFP-U6 sgRNA vector was constructed from a
522 pMSCV-CD19 scFv-IRES-RFP vector provided by laboratory of Dr. Feng Shao
523 (National Institute of Biological Sciences, Beijing). An U6 sgRNA cassette was
524 assembled by seamless cloning kit (Biomed, CL116).

525 $CD8^+$ T-cells were purified from splenocytes of Cas9-EGFP knock-in mice by a mouse
526 $CD8^+$ T-cell isolation kit (R&D, MAGM203). At day 0, $CD8^+$ T-cells were stimulated with
527 anti-CD3 (1 μg/ml, Cat#14-0031-86) and anti-CD28 (0.5 μg/ml, Cat#102116) in
528 complete RPMI 1640 medium containing 20 ng/ml IL2 for 24 hours. On day 1, activated
529 $CD8^+$ T-cells were enriched by Percoll isolation and spin-infected (2,000 g, 30 °C, 1
530 hour, with no acceleration or brake) with retrovirus expressing anti-CD19-CAR and
531 sgRNA supplemented with polybrene (8 μg/ml) in 24-well-plate. The RFP^+ cells were
532 sorted on day 3 for further culture. $CD8^+$ T-cells were cultured with the same condition
533 as T memory cells. In vitro killing assay was perform on day 7 by mixing anti-CD19-
534 CAR-T-cells with Nalm6.

535 NY-ESO-1 specific TCR (1G4)[29] was synthesized and cloned into a lentiviral

536 backbone with a SFFV promoter. T2A-BFP fragment and U6 shRNA cassette were
537 assembled by seamless cloning kit (Biomed, CL116) simultaneously.

538 NY-ESO-1 specific TCR-T-cells were generated following the human $CD8^+$ T-cell
539 isolation, culture, and transduction protocols. 3 days post-transduction, BFP^+ cells
540 were sorted for further culture. 7 days post-transduction, in vitro killing assay was
541 performed by mixing T-cells with A375 cells.

542 **CRISPR/Cas9 screening**

543 For ex vivo PD-1 expression screening, at Day 6, $3x10^6$ B16F10-OVA cells were plated
544 in 15 cm dishes in DMEM (DMEM+10% FBS+ Pen/Strep). On Day 7, puromycin-
545 selected OT-I T-cells were resuspended in a final concentration of $6x10^5$ cells/ml with
546 complete RPMI 1640 medium supplemented with IL2 (2 ng/ml), IL7 (2.5 ng/ml), and
547 IL15 (10 ng/ml), and added to B16F10-OVA cells at a T-cell:B16F10-OVA cell ratio of
548 4:1. Cells were co-cultured overnight at 37 °C. $CD8^+$ T-cells were then collected and
549 stained with PE anti-PD-1 in 2% FBS/PBS for 30 minutes on ice. The highest and
550 lowest 5% $PD\text{-}1^+$ cells were sorted via BD FACSAria.

551 For the secondary small custom library in vivo screening, following 4-day puromycin
552 selection, an aliquot of $2x10^6$ infected OT-I T-cells was saved as input (approximately
553 269X cell coverage per sgRNA). Library-infected OT-I T-cells ($2x10^6$ cells per recipient)
554 were intravenously transferred into mice bearing Day 14 B16F10-OVA tumors. In total,
555 24 mice were used as recipients. At 7 days post-adoptive transfer, B16F10-OVA
556 tumors were digested into single-cell suspensions, and tumor-infiltrated $CD8^+$ T-cells
557 were isolated by biotin anti-mouse CD8a (Biolegend, 100704) and streptavidin beads.
558 Meanwhile, a 1/20 volume aliquot of single-cell suspension was used for OT-I staining
559 to estimate numbers of infiltrated OT-I T-cells in each tumor. A total of $1x10^4$ to 1×10^5
560 OT-I T-cells were collected per tumor.

561 **Sequencing library preparation**

562 Genomic DNA was extracted by phenol/chloroform extraction. Primary PCR was

563 performed using Titanium Taq DNA Polymerase (Clontech, 639242) to amplify the
564 sgRNA region. A secondary PCR was performed to add adaptors and indexes to each
565 sample. Nova-seq 150-bp paired-end sequencing (Illumina) was performed.

566 **Analysis of screening results**

567 Raw reads were preprocessed using sequence-grooming tools to remove adaptor
568 sequences with Cutadapt (version 3.4)[48] and to merge reads with FLASH (version
569 1.2.11)[49]. Then, MAGeCK (version 0.5.9.5)[50] was used to analyze the screening data.
570 Specifically, the MAGeCK "count" command was employed to generate read counts
571 for all samples, which were subsequently merged into a count matrix. The MAGeCK
572 "test" command was then used to identify the top negatively and positively selected
573 gRNAs or genes, using default settings. The software is available from
574 https://sourceforge.net/projects/mageck/. Additionally, Gene Set Enrichment Analysis
575 (GSEA) in the Kyoto Encyclopedia of Genes and Genomes (KEGG) functional
576 pathway was performed using the GSEA() function from the R package clusterProfiler
577 (version 3.12.0)[51], with default parameters. The KEGG database was selected from
578 the "C2" category of the R package msigdbr (version 7.5.1), available at
579 https://igordot.github.io/msigdbr/.

580 **Flow cytometry**

581 For surface staining, cells were stained in 2% FBS/PBS on ice for 30 minutes.
582 Intracellular staining was performed with a fixation/permeabilization kit (BD
583 Biosciences) according to manufacturer's instructions. The following antibodies were
584 used: APC anti-mouse CD8a (Invitrogen, 17-0081-83), PE anti-mouse CD279 (PD-1)
585 (BioLegend, 109104), APC anti-mouse CD279 (PD-1) (BioLegend, 109112), PE-
586 streptavidin (BioLegend, 405203), biotinylated erythrina cristagalli lectin (ECL) (B-
587 1145-5), biotinylated succinylated wheat germ agglutinin (sWGA) (B-1025S-5),
588 biotinylated recombinant Gal-1, APC anti-human CD8a (BioLegend, 300912). Flow
589 cytometry was performed by BD FACSAria and data were analyzed with FlowJo.

590 **ELISA**

591 OT-I T-cells ($3x10^5$/ml) were co-cultured with B16F10-OVA cells at 37 °C for 8 hours
592 in the presence of IL2 (2 ng/ml), IL7 (2.5 ng/ml), and IL15 (10 ng/ml). Supernatants
593 were collected after co-culture. TNFα and IFNγ in the culture supernatant were
594 measured using ELISA kits (ABclonal, Cat#RK00027, Cat#RK00019). Samples were
595 plated in duplicate.

596 Human $CD8^+$ T-cells (3×10^5/ml) were co-cultured with A375 cells at 37 °C for 24 hours
597 in the presence of human IL2 (500 IU/ml). Supernatants were collected for
598 measurement of TNFα and IFNγ secretion using ELISA kits (ABclonal, Cat#RK00030,
599 Cat#RK00015).

600 **Mouse tumor models and adoptive transfer experiments**

601 $4x10^5$ B16F10-OVA cells were injected subcutaneously into female C57BL/6J mice.
602 Seven days post-injection, mice bearing tumors of similar size were randomly
603 separated into 2 groups. A total of $2x10^6$ *B4galt1* gRNA-transduced or control gRNA-
604 transduced OT-I T-cells were injected intravenously. Tumors were then measured
605 every two days with an electronic digital caliper. Tumor volume was calculated as width
606 x width x length x 1/2.

607 **Tumor-infiltrated lymphocyte (TIL) isolation**

608 B16F10-OVA tumors were cut into small pieces in 6-well plates containing 5 ml RPMI
609 1640, 2% FBS, and 50 U/ml collagenase type IV (Invitrogen, V900893). Samples were
610 incubated at 37 ℃ for 1 hour with rotation. Suspensions were passed through a 70 μm
611 strainer and washed three times with PBS. Samples were then used for antibody
612 staining and FACS analysis.

613 **T-cell infiltration and proliferation within tumors**

614 Following 4-day puromycin selection, infected OT-I T-cells were labeled with CFSE
615 (carboxyfluorescein diacetate succinimidyl ester, Invitrogen), and $2x10^6$ labeled cells

616 were intravenously transferred into Day 14 B16F10-OVA tumor-bearing mice. CFSE
617 dilution was quantified by flow cytometry at 24 hours and Day 6 following transfer.

618 **In vitro targeted cell killing**

619 For OT-I T-cell killing activity assay, B16F10-OVA cells and B16F10 cells were labeled
620 as $CFSE^{hi}$ (2.5 μM) and $CFSE^{lo}$ (50 nM), respectively, and then co-cultured with OT-I
621 T-cells in 96-well plates at the indicated ratios. Cancer cells without addition of OT-I T-
622 cells were used as controls. Following 24 hours of incubation, the ratios of $CFSE^{hi}$ and
623 $CFSE^{lo}$ populations were detected by FACS.

624 Specific killing was calculated by following equation: specific killing percentage = [1-
625 ($CFSE^{hi}$/$CFSE^{lo}$ of T-cell)/($CFSE^{hi}$/$CFSE^{lo}$ of cancer cell only)] × 100%.

626 For NY-ESO-1 TCR-T and hCD19-CAR-T-cell in vitro killing assays, A375 cells and
627 Nalm6 cells were co-cultured with T-cells for 24h and 8h, respectively. The killing
628 percentage was calculated by following equation: killing percentage = [1-(survived
629 target cell number / survived target cell number in non-T-cell wells)] × 100%.

630

631 **Proteomic analysis of Gal-1 binding proteins in $CD8^+$ T-cells**

632 Recombinant Gal-1 was purified[52] and coupled with sepharose beads (Cat#GE17-
633 0906-01). *B4galt1* knockout OT-I T-cells were co-cultured with MC38 for 8 hours and
634 then stained by anti-Gal-1 antibody for sorting of Gal-1 negative OT-I T-cell population.
635 Membrane extracts of OT-I T-cells were prepared by Mem-PER™ Plus Kit
636 (Cat#89842Y). Extracts were incubated with Gal-1-sepharose beads. After washing,
637 binding proteins were eluted by 20 mM lactose and precipitated by DOC/TCA, and
638 then separated on SDS-PAGE followed by silver staining (Sigma, PROTSIL1). The
639 samples were digested and subjected to LC-MS (LTQ ORBITRAP Velos mass
640 spectrometer, Thermo Fisher Scientific, San Jose, CA, USA).

641 Raw data was processed by Proteome Discoverer (version1.4,

642 https://www.thermofisher.com/hk/en/home/industrial/mass-spectrometry/liquid-
643 chromatography-mass-spectrometry-lc-ms/lc-ms-software/multi-omics-data-
644 analysis/proteome-discoverer-software.html) to obtain a PSM (peptide spectrum
645 matches) raw intensity table of all identified proteins for further analysis with R package
646 DEqMS[53]. Raw intensity values were log2 transformed, and for each PSM, the median
647 of log2 intensity was subtracted to get a relative log2 ratio. Then different expression
648 of protein calculation was enabled in eBayes() function with method ROC (receiver
649 operating characteristic) analysis. Differentially expressed proteins were selected by
650 criteria $P < 0.05$. Those proteins were used for functional enrichment analysis with R
651 package ClusterProfiler (version 3.12.0)[54] .

652 **Western blot**

653 10 μg cell membrane extracts of OT-I T-cells were separated by SDS-PAGE gels. Gels
654 were transferred to nitrocellulose membranes (Amersham™ Protran®,
655 Cat#10600001). Anti-CD8b (Abcam, Cat# ab228965) (1:1000), Anti-Ly9 (Abcam, Cat#
656 ab252931) (1:1000), anti-Igf2g (Sino Biological, Cat# 107533-T40) (1:500), anti-Itgal
657 (Solarbio, Cat# K002895P) (1:500), anti-Itgb7 (Solarbio, Cat#K004272P) (1:500), anti-
658 Lnpep (Santa Cruz, Cat#sc-365300) (1:100), and anti-Sell (Santa Cruz, Cat#sc-
659 390756) (1:100) were used as primary antibodies. Secondary antibodies were IRDye®
660 680RD Donkey anti-Mouse IgG (LI-COR, P/N 926-68072) (1:10000), IRDye® 800CW
661 Goat anti-Mouse IgG (LI-COR, P/N 926–32210) (1:10000), IRDye® 680RD Goat anti-
662 Rabbit IgG (LI-COR, P/N 926-68071) (1:10000), IRDye® 800CW Goat anti-Rabbit IgG
663 (LI-COR, P/N 926-32211) (1:10000). The membranes were scanned on an Odyssey
664 imager (LI-COR).

665 **FRET**

666 TCR-CD8 FRET was measured by flow cytometry[30]. T-cells were incubated with PE-
667 anti-Vα2 and APC-anti-CD8α at 4℃ for 30 minutes. Samples were stained with either
668 antibody, both or neither. After staining, samples were fixed with fixation buffer at 4℃

669 for 10 minutes. FRET emission was assessed and FRET efficiency was calculated in
670 FRET units as reported previously[30].

671 **RT-qPCR and RNA-Seq**

672 Total RNA was extracted using TRIzol® Reagent (Ambion, Cat# 15596018). cDNA
673 was synthesized by the ImProm-II™ Reverse Transcriptase system (Promega, Cat#
674 A3801) using 100 ng RNA per reaction. The qPCR reactions were prepared with TB
675 Green® Premix Ex Taq™ (Takara, Cat# RR420A) using 1 µl cDNA per reaction in a
676 20 µl reaction volume. The relative gene expression levels were normalized to GAPDH.

677 Total RNA was used as input material for the RNA sample preparations. Sequencing
678 libraries were generated using NEBNext Ultra RNA Library Prep Kit for Illumina (NEB,
679 Catalog #E7530L) following manufacturer's recommendations and index codes were
680 added to attribute sequences to each sample. Prepared libraries were quantified and
681 sequenced by the Illumina NovaSeq 6000 S4 platform with 150 bp paired-end reads.

682 **RNA-Seq data analysis**

683 Raw data was aligned to mouse reference genome (mm10) with Ensemble version 98
684 gene annotation using TopHat2 (version 2.1.1). The raw count of each gene was then
685 calculated using HTSeq (version 1.99.2)[55] and normalized to Fragments Per Kilobase
686 of transcript per Million mapped reads (FPKM) by cufflinks (version 2.2.1)[56].
687 Differential gene expression analysis was performed using the R-based toolkit
688 DESeq2 (version 1.38.0)[57], with differentially expressed genes (DEGs) defined by a
689 significance threshold of $P < 0.05$ or $P < 0.01$. Functional enrichment analysis of these
690 DEGs was conducted using the R package ClusterProfiler (version 3.12.0)[54].

691 **Statistical analysis**

692 Statistical analyses were conducted using R 4.1.0. Unless otherwise stated, statistical
693 significance was determined using a two-tailed paired Student's t-test (*$P < 0.05$, **P
694 < 0.01, ***$P < 0.001$; NS, not significant) with the function t.test(). Two-way ANOVA

695 was performed using the function aov(). In the figures, the mean and standard error of
696 the mean (SEM) are presented, with error bars representing the SEM value, calculated
697 using the function sem().

698 **Supplemental information**

699 Supplemental information includes 6 figures and 5 tables.

700 **Figure S1. Multiple components in N-glycan biosynthesis pathway were identified in**
701 **genome-wide screenings for PD-1 regulators in CD8$^+$ T-cells.**

702 a. Schematic views of the N-glycan biosynthesis pathway. The genes identified in
703 current genome-wide screenings are labeled.
704 b. Distribution of N-glycan biosynthesis-related genes in current screenings. The blue
705 curve represents all target genes; the red curve represents all genes involved in
706 the N-glycan biosynthesis pathway; and the gray curve represents control gRNAs.
707 c. Representative PD-1 FACS plots for gRNAs targeting B4galt1, Mgat2, and Dpm3
708 genes.

709 **Figure S2. Effect of B4GALT1 knockout on functions of hCD19-CAR-T-cells and**
710 **anti-CD3/28 stimulated T-cells.**

711 a. CRISPR/Cas9 knockout of B4GALT1 in hCD19-CAR-T-cells does not affect in vitro
712 killing of Nalm6 target cells.

713 Data are shown as the mean ± SEM. NS, not significant.

714 **Figure S3. Effect of B4GALT1 knockout on functions of anti-CD3/28 stimulated**
715 **T-cells.**

716 a. B4GALT1 knockout and control OT-I T-cells (1X10^5 cells/ml) were stimulated with
717 anti-CD3 (1 mg/ml) and anti-CD28 (0.5 mg/ml) for 8 hours. The mRNA expression
718 levels of Tnfα and Ifnγ were measured by quantitative RT-qPCR. The p-value was
719 calculated using a two-tailed Student's t-test.

720 Data are shown as the mean ± SEM. **P < 0.01. NS, not significant.

721 **Figure S4. Effect of B4GALT1 knockout on functions of tumor-infiltrated OT-I T-**
722 **cells.**

723 a. Tumor infiltration of CFSE-labeled OT-I $CD8^+$ T-cells 24 hours after transplantation.
724 The p-value was calculated using a two-tailed Student's t-test.
725 b. Enhanced proliferation of CFSE-labeled B4GALT1 knockout (sgB4galt1) OT-I T-
726 cells in tumors.

727 Data are shown as the mean ± SEM. NS, not significant.

728 **Figure S5. CRISPR/Cas9 knockout of B4GALT1 in OT-I T-cells alters surface-**
729 **binding of lectins and galectin-1.**

730 a. Scheme for FACS analysis of N-glycome by lectins and galectin-1.

731 b-d. Cells were stained with biotin-ECL (b), biotin-sWGA (c), biotin-rGal-1 (d) and
732 streptavidin-PE. Blue and red curves indicate control sgRNA- and sgB4galt1-
733 infected OT-I cells, respectively. Gray dotted curves indicate cells stained with
734 streptavidin-PE only. The MFIs of each sample were measured by FACS. The p-
735 value was calculated using a two-tailed Student's t-test.

736 Data are shown as the mean ± SEM. *P < 0.05; **P < 0.01.

737 **Figure S6. Expression levels of B4GALT1 and tumor-infiltrated $CD8^+$ T-cells in**
738 **tumor microenvironment are associated with prognosis of human patients.**

739 a. Kaplan-Meier survival curves of B4GALT1 expression levels for all primary tumor
740 samples in TCGA cohort.
741 b. Kaplan-Meier survival curves of CD8A normalized B4GALT1 expression levels for
742 all primary tumor samples in TCGA cohort.
743 c. The p-value heatmap showing associations between B4GALT1 expression levels
744 and overall survival of patients with different tumor CD8A levels ($CD8A^{high}$ and
745 $CD8A^{low}$) in indicated TCGA cohorts (three columns on the left), as well as
746 associations between CD8A expression levels and overall survival of patients with

747 different tumor B4GALT1 levels (B4GALT1^{high} and B4GATL1^{low}) in indicated TCGA
748 cohorts (three columns on the right). Hazard ratio (HR) values are listed in boxes.
749 Samples with p-value > 0.05 were all filled with white background.

750 The p-values for all survival curves were calculated using two-sided Log-rank test.

751

752 **Supplementary Table 1. List of sequences of gRNAs and primers used in current**
753 **study.**

754 **Supplementary Table 2. List of plasmids used in current study.**

755 **Supplementary Table 3. Information of custom library used in current study.**

756 **Supplementary Table 4. Results of ex vivo CRISPR/Cas9 genome-wide**
757 **screenings in Fig1b.**

758 **Supplementary Table 5. Results of in vivo CRISPR/Cas9 screenings with custom**
759 **library in Fig2c.**

References

1. Spencer KR, Wang J, Silk AW, et al. *Biomarkers for Immunotherapy: Current Developments and Challenges[J].* Am Soc Clin Oncol Educ Book, 2016. 35: p. e493-503.
2. Havel JJ, Chowell D,Chan TA. *The evolving landscape of biomarkers for checkpoint inhibitor immunotherapy[J].* Nat Rev Cancer, 2019. 19(3): p. 133-150.
3. Hodi FS, Mihm MC, Soiffer RJ, et al. *Biologic activity of cytotoxic T lymphocyte-associated antigen 4 antibody blockade in previously vaccinated metastatic melanoma and ovarian carcinoma patients[J].* Proc Natl Acad Sci U S A, 2003. 100(8): p. 4712-4717.
4. Brahmer JR, Tykodi SS, Chow LQ, et al. *Safety and activity of anti-PD-L1 antibody in patients with advanced cancer[J].* N Engl J Med, 2012. 366(26): p. 2455-2465.
5. Topalian SL, Hodi FS, Brahmer JR, et al. *Safety, activity, and immune correlates of anti-PD-1 antibody in cancer[J].* N Engl J Med, 2012. 366(26): p. 2443-2454.
6. Ribas A,Wolchok JD. *Cancer immunotherapy using checkpoint blockade[J].* Science, 2018. 359(6382): p. 1350-1355.
7. Cercek A, Lumish M, Sinopoli J, et al. *PD-1 Blockade in Mismatch Repair-Deficient, Locally Advanced Rectal Cancer[J].* N Engl J Med, 2022.
8. June CH, O'Connor RS, Kawalekar OU, et al. *CAR T cell immunotherapy for human cancer[J].* Science, 2018. 359(6382): p. 1361-1365.
9. Rafiq S, Hackett CS,Brentjens RJ. *Engineering strategies to overcome the current roadblocks in CAR T cell therapy[J].* Nat Rev Clin Oncol, 2020. 17(3): p. 147-167.
10. Agata Y, Kawasaki A, Nishimura H, et al. *Expression of the PD-1 antigen on the surface of stimulated mouse T and B lymphocytes[J].* Int Immunol, 1996. 8(5): p. 765-772.
11. Yu Y, Tsang JC, Wang C, et al. *Single-cell RNA-seq identifies a PD-1(hi) ILC progenitor and defines its development pathway[J].* Nature, 2016. 539(7627): p. 102-106.
12. Gordon SR, Maute RL, Dulken BW, et al. *PD-1 expression by tumour-associated macrophages inhibits phagocytosis and tumour immunity[J].* Nature, 2017. 545(7655): p. 495-499.
13. Park BV, Freeman ZT, Ghasemzadeh A, et al. *TGFbeta1-Mediated SMAD3 Enhances PD-1 Expression on Antigen-Specific T Cells in Cancer[J].* Cancer Discov, 2016. 6(12): p. 1366-1381.
14. Stephen TL, Payne KK, Chaurio RA, et al. *SATB1 Expression Governs Epigenetic Repression of PD-1 in Tumor-Reactive T Cells[J].* Immunity, 2017. 46(1): p. 51-64.
15. Okada M, Chikuma S, Kondo T, et al. *Blockage of Core Fucosylation Reduces Cell-Surface Expression of PD-1 and Promotes Anti-tumor Immune Responses of T Cells[J].* Cell Rep, 2017. 20(5): p. 1017-1028.
16. Meng X, Liu X, Guo X, et al. *FBXO38 mediates PD-1 ubiquitination and regulates anti-tumour immunity of T cells[J].* Nature, 2018. 564(7734): p. 130-135.
17. Zhou XA, Zhou J, Zhao L, et al. *KLHL22 maintains PD-1 homeostasis and prevents excessive T cell suppression[J].* Proc Natl Acad Sci U S A, 2020. 117(45): p. 28239-28250.

18. Wei J, Long L, Zheng W, et al. *Targeting REGNASE-1 programs long-lived effector T cells for cancer therapy[J].* Nature, 2019. 576(7787): p. 471-476.
19. Zhao H, Liu Y, Wang L, et al. *Genome-wide fitness gene identification reveals Roquin as a potent suppressor of CD8 T cell expansion and anti-tumor immunity[J].* Cell Rep, 2021. 37(10): p. 110083.
20. Ma X, Xiao L, Liu L, et al. *CD36-mediated ferroptosis dampens intratumoral CD8(+) T cell effector function and impairs their antitumor ability[J].* Cell Metab, 2021. 33(5): p. 1001-1012 e1005.
21. Xu S, Chaudhary O, Rodriguez-Morales P, et al. *Uptake of oxidized lipids by the scavenger receptor CD36 promotes lipid peroxidation and dysfunction in CD8(+) T cells in tumors[J].* Immunity, 2021. 54(7): p. 1561-1577 e1567.
22. Rodeheffer C,Shur BD. *Targeted mutations in beta1,4-galactosyltransferase I reveal its multiple cellular functions[J].* Biochim Biophys Acta, 2002. 1573(3): p. 258-270.
23. Cheng X, Wang X, Han Y, et al. *The expression and function of beta-1,4-galactosyltransferase-I in dendritic cells[J].* Cell Immunol, 2010. 266(1): p. 32-39.
24. Han Y, Zhou X, Ji Y, et al. *Expression of beta-1,4-galactosyltransferase-I affects cellular adhesion in human peripheral blood CD4+ T cells[J].* Cell Immunol, 2010. 262(1): p. 11-17.
25. Gomez-Henao W, Tenorio EP, Sanchez FRC, et al. *Relevance of glycans in the interaction between T lymphocyte and the antigen presenting cell[J].* Int Rev Immunol, 2021. 40(4): p. 274-288.
26. Cui Y, Li J, Zhang P, et al. *B4GALT1 promotes immune escape by regulating the expression of PD-L1 at multiple levels in lung adenocarcinoma[J].* J Exp Clin Cancer Res, 2023. 42(1): p. 146.
27. Hsu TH, Chang YC, Lee YY, et al. *B4GALT1-dependent galectin-8 binding with TGF-beta receptor suppresses colorectal cancer progression and metastasis[J].* Cell Death Dis, 2024. 15(9): p. 654.
28. De Vitis C, Corleone G, Salvati V, et al. *B4GALT1 Is a New Candidate to Maintain the Stemness of Lung Cancer Stem Cells[J].* J Clin Med, 2019. 8(11).
29. Robbins PF, Li YF, El-Gamil M, et al. *Single and dual amino acid substitutions in TCR CDRs can enhance antigen-specific T cell functions[J].* J Immunol, 2008. 180(9): p. 6116-6131.
30. Smith LK, Boukhaled GM, Condotta SA, et al. *Interleukin-10 Directly Inhibits CD8(+) T Cell Function by Enhancing N-Glycan Branching to Decrease Antigen Sensitivity[J].* Immunity, 2018. 48(2): p. 299-312 e295.
31. Borger JG, Zamoyska R,Gakamsky DM. *Proximity of TCR and its CD8 coreceptor controls sensitivity of T cells[J].* Immunol Lett, 2014. 157(1-2): p. 16-22.
32. Weinstein JN, Collisson EA, Mills GB, et al. *The Cancer Genome Atlas Pan-Cancer analysis project[J].* Nat Genet, 2013. 45(10): p. 1113-1120.
33. Tang Z, Kang B, Li C, et al. *GEPIA2: an enhanced web server for large-scale expression profiling and interactive analysis[J].* Nucleic Acids Res, 2019. 47(W1): p. W556-W560.
34. Pan YM,Cheng YX. *Splicing factor proline- and glutamine-rich regulates cytotoxic T*

lymphocytes-mediated cytotoxicity on non-small cell lung cancer by directly binding to PD-L1 3'UTR[J]. Medicine, 2023. 102(45).

35. Coulie PG, Van den Eynde BJ, van der Bruggen P, et al. *Tumour antigens recognized by T lymphocytes: at the core of cancer immunotherapy[J].* Nature Reviews Cancer, 2014. 14(2): p. 135-146.

36. Keir ME, Butte MJ, Freeman GJ, et al. *PD-1 and its ligands in tolerance and immunity[J].* Annu Rev Immunol, 2008. 26: p. 677-704.

37. Frontiers Production O. *Erratum: CD8 T cell function and cross-reactivity explored by stepwise increased peptide-HLA versus TCR affinity[J].* Front Immunol, 2023. 14: p. 1178295.

38. Kinter AL, Godbout EJ, McNally JP, et al. *The common gamma-chain cytokines IL-2, IL-7, IL-15, and IL-21 induce the expression of programmed death-1 and its ligands[J].* J Immunol, 2008. 181(10): p. 6738-6746.

39. Dong H, Zhu G, Tamada K, et al. *B7-H1, a third member of the B7 family, co-stimulates T-cell proliferation and interleukin-10 secretion[J].* Nat Med, 1999. 5(12): p. 1365-1369.

40. Abdelbary M,Nolz JC. *N-linked glycans: an underappreciated key determinant of T cell development, activation, and function[J].* Immunometabolism (Cobham), 2023. 5(4): p. e00035.

41. Kalos M,June CH. *Adoptive T cell transfer for cancer immunotherapy in the era of synthetic biology[J].* Immunity, 2013. 39(1): p. 49-60.

42. Kamphorst AO,Ahmed R. *CD4 T-cell immunotherapy for chronic viral infections and cancer[J].* Immunotherapy, 2013. 5(9): p. 975-987.

43. Sterner RC,Sterner RM. *CAR-T cell therapy: current limitations and potential strategies[J].* Blood Cancer J, 2021. 11(4): p. 69.

44. Zhang T, Tai Z, Miao F, et al. *Adoptive cell therapy for solid tumors beyond CAR-T: Current challenges and emerging therapeutic advances[J].* J Control Release, 2024. 368: p. 372-396.

45. Wu R, Forget MA, Chacon J, et al. *Adoptive T-cell therapy using autologous tumor-infiltrating lymphocytes for metastatic melanoma: current status and future outlook[J].* Cancer J, 2012. 18(2): p. 160-175.

46. Platt RJ, Chen S, Zhou Y, et al. *CRISPR-Cas9 knockin mice for genome editing and cancer modeling[J].* Cell, 2014. 159(2): p. 440-455.

47. Kurachi M, Kurachi J, Chen Z, et al. *Optimized retroviral transduction of mouse T cells for in vivo assessment of gene function[J].* Nat Protoc, 2017. 12(9): p. 1980-1998.

48. Martin M. *Cutadapt removes adapter sequences from high-throughput sequencing reads[J].* EMBnet. journal, 2011. 17(1): p. 10-12.

49. Magoc T,Salzberg SL. *FLASH: fast length adjustment of short reads to improve genome assemblies[J].* Bioinformatics, 2011. 27(21): p. 2957-2963.

50. Li W, Xu H, Xiao T, et al. *MAGeCK enables robust identification of essential genes from genome-scale CRISPR/Cas9 knockout screens[J].* Genome Biol, 2014. 15(12): p. 554.

51. Yu G, Wang L-G, Han Y, et al. *clusterProfiler: an R package for comparing biological*

themes among gene clusters[J]. Omics: a journal of integrative biology, 2012. 16(5): p. 284-287.

52. Prato CA, Carabelli J, Cattaneo V, et al. *Purification of recombinant galectins expressed in bacteria[J].* STAR protocols, 2020. 1(3): p. 100204.
53. Zhu Y, Orre LM, Zhou Tran Y, et al. *DEqMS: A Method for Accurate Variance Estimation in Differential Protein Expression Analysis[J].* Mol Cell Proteomics, 2020. 19(6): p. 1047-1057.
54. Wu T, Hu E, Xu S, et al. *clusterProfiler 4.0: A universal enrichment tool for interpreting omics data[J].* Innovation (Camb), 2021. 2(3): p. 100141.
55. Putri GH, Anders S, Pyl PT, et al. *Analysing high-throughput sequencing data in Python with HTSeq 2.0[J].* Bioinformatics, 2022. 38(10): p. 2943-2945.
56. Trapnell C, Roberts A, Goff L, et al. *Differential gene and transcript expression analysis of RNA-seq experiments with TopHat and Cufflinks[J].* Nat Protoc, 2012. 7(3): p. 562-578.
57. Love MI, Huber W,Anders S. *Moderated estimation of fold change and dispersion for RNA-seq data with DESeq2[J].* Genome Biol, 2014. 15(12): p. 550.

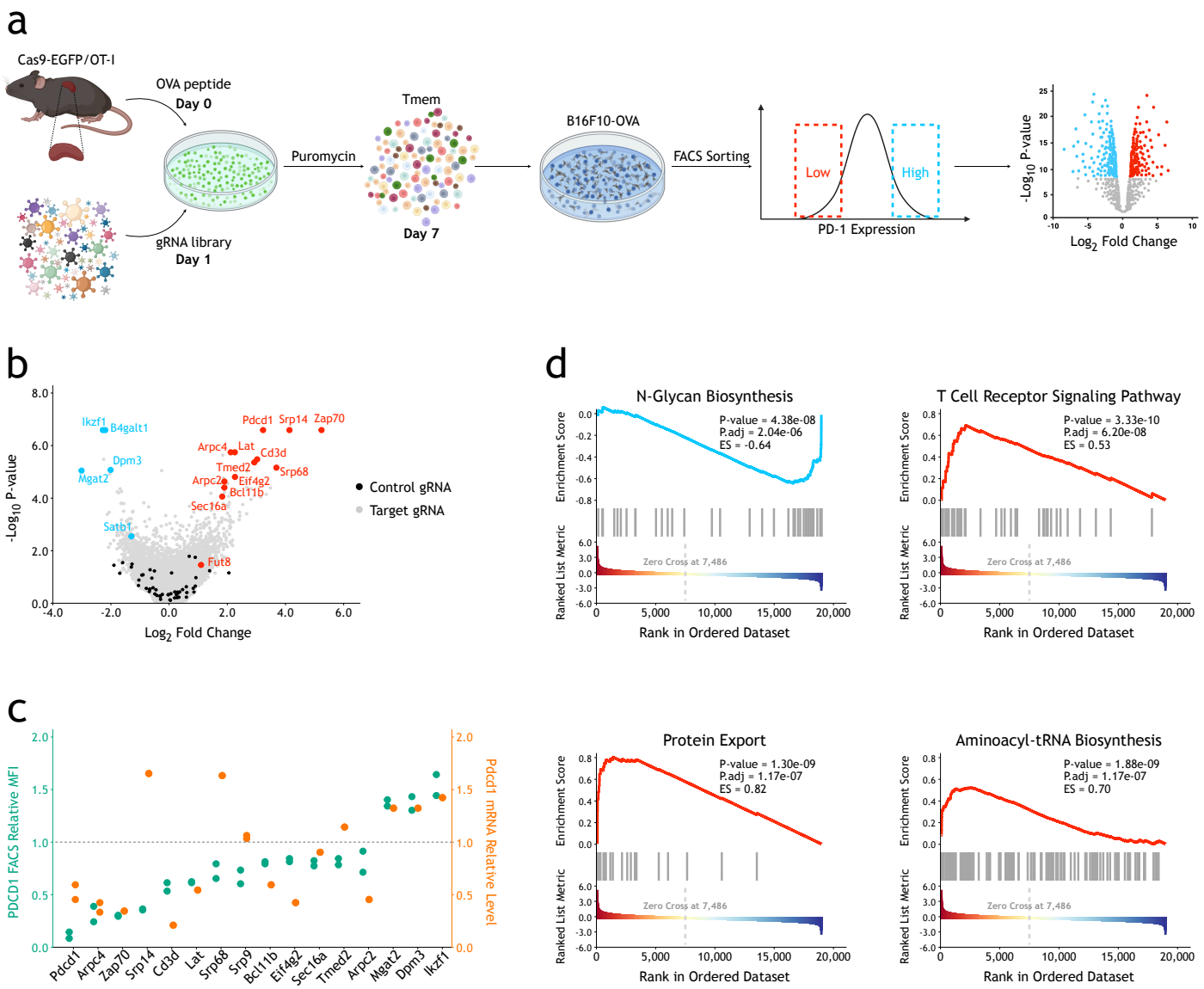
a
Cas9-EGFP/OT-I
OVA peptide
Day 0
gRNA library
Day 1
Puromycin
Tmem
Day 7
B16F10-OVA
FACS Sorting
Low
High
PD-1 Expression
-Log10 P-value
Log2 Fold Change
b
-Log10 P-value
Log2 Fold Change
Ikzf1
B4galt1
Dpm3
Mgat2
Satb1
Pdcd1
Srp14
Zap70
Arpc4
Lat
Cd3d
Tmed2
Srp68
Arpc2
Eif4g2
Bcl11b
Sec16a
Fut8
Control gRNA
Target gRNA
c
PDCD1 FACS Relative MFI
Pdcd1 mRNA Relative Level
Pdcd1
Arpc4
Zap70
Srp14
Cd3d
Lat
Srp68
Srp9
Bcl11b
Eif4g2
Sec16a
Tmed2
Arpc2
Mgat2
Dpm3
Ikzf1
d
N-Glycan Biosynthesis
P-value = 4.38e-08
P.adj = 2.04e-06
ES = -0.64
T Cell Receptor Signaling Pathway
P-value = 3.33e-10
P.adj = 6.20e-08
ES = 0.53
Protein Export
P-value = 1.30e-09
P.adj = 1.17e-07
ES = 0.82
Aminoacyl-tRNA Biosynthesis
P-value = 1.88e-09
P.adj = 1.17e-07
ES = 0.70
Enrichment Score
Ranked List Metric
Zero Cross at 7,486
Rank in Ordered Dataset

Figure 1

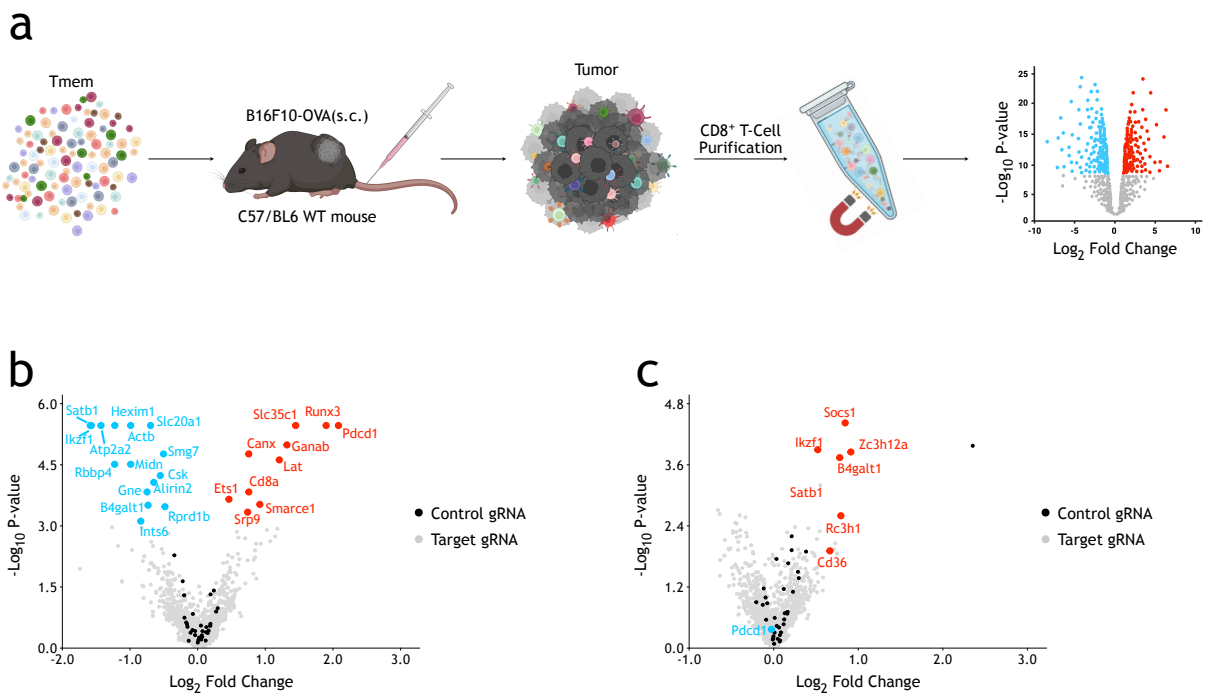
a
Tmem
B16F10-OVA(s.c.)
C57/BL6 WT mouse
Tumor
CD8+ T-Cell
Purification
-Log10 P-value
Log2 Fold Change
b
Satb1
Hexim1
Slc20a1
Ikzf1
Actb
Atp2a2
Smg7
Rbbp4
Midn
Csk
Gne
Alirin2
B4galt1
Rprd1b
Ints6
Slc35c1
Runx3
Pdcd1
Canx
Ganab
Lat
Cd8a
Ets1
Smarce1
Srp9
Control gRNA
Target gRNA
-Log10 P-value
Log2 Fold Change
c
Socs1
Ikzf1
Zc3h12a
B4galt1
Satb1
Rc3h1
Cd36
Pdcd1
Control gRNA
Target gRNA
-Log10 P-value
Log2 Fold Change

Figure 2

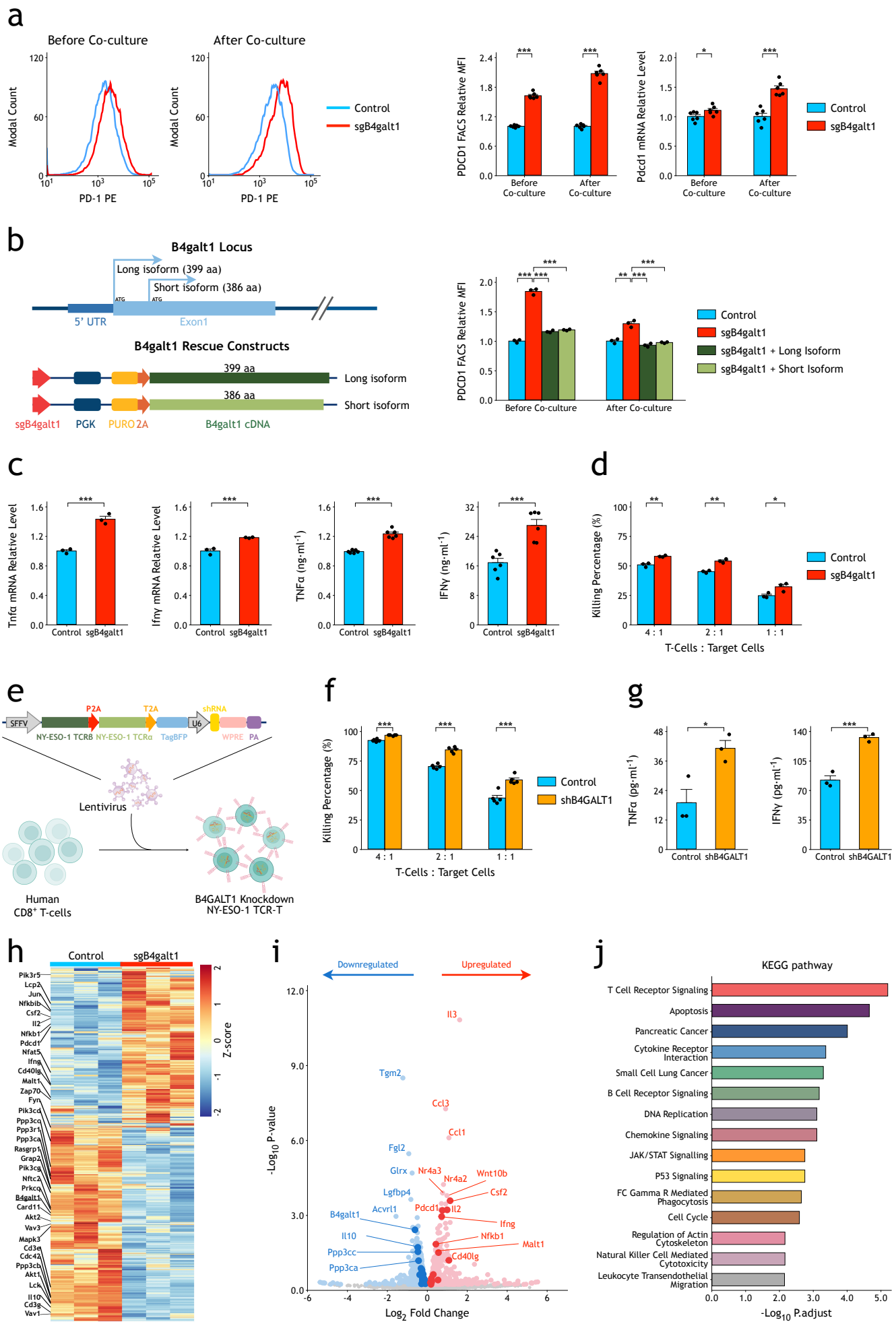
a
Before Co-culture
After Co-culture
Modal Count
PD-1 PE
Control
sgB4galt1
PDCD1 FACS Relative MFI
Pdcd1 mRNA Relative Level
Before Co-culture
After Co-culture
b
B4galt1 Locus
Long isoform (399 aa)
Short isoform (386 aa)
5' UTR
Exon1
B4galt1 Rescue Constructs
399 aa
386 aa
Long isoform
Short isoform
sgB4galt1
PGK
PURO 2A
B4galt1 cDNA
sgB4galt1 + Long Isoform
sgB4galt1 + Short Isoform
c
Tnfα mRNA Relative Level
Ifnγ mRNA Relative Level
TNFα (ng·ml⁻¹)
IFNγ (ng·ml⁻¹)
d
Killing Percentage (%)
T-Cells : Target Cells
e
SFFV
P2A
T2A
shRNA
U6
NY-ESO-1 TCRB
NY-ESO-1 TCRα
TagBFP
WPRE
PA
Lentivirus
Human CD8⁺ T-cells
B4GALT1 Knockdown NY-ESO-1 TCR-T
f
shB4GALT1
g
h
Z-score
i
Downregulated
Upregulated
-Log10 P-value
Log2 Fold Change
j
KEGG pathway
T Cell Receptor Signaling
Apoptosis
Pancreatic Cancer
Cytokine Receptor Interaction
Small Cell Lung Cancer
B Cell Receptor Signaling
DNA Replication
Chemokine Signaling
JAK/STAT Signalling
P53 Signaling
FC Gamma R Mediated Phagocytosis
Cell Cycle
Regulation of Actin Cytoskeleton
Natural Killer Cell Mediated Cytotoxicity
Leukocyte Transendothelial Migration
-Log10 P.adjust

Figure 3

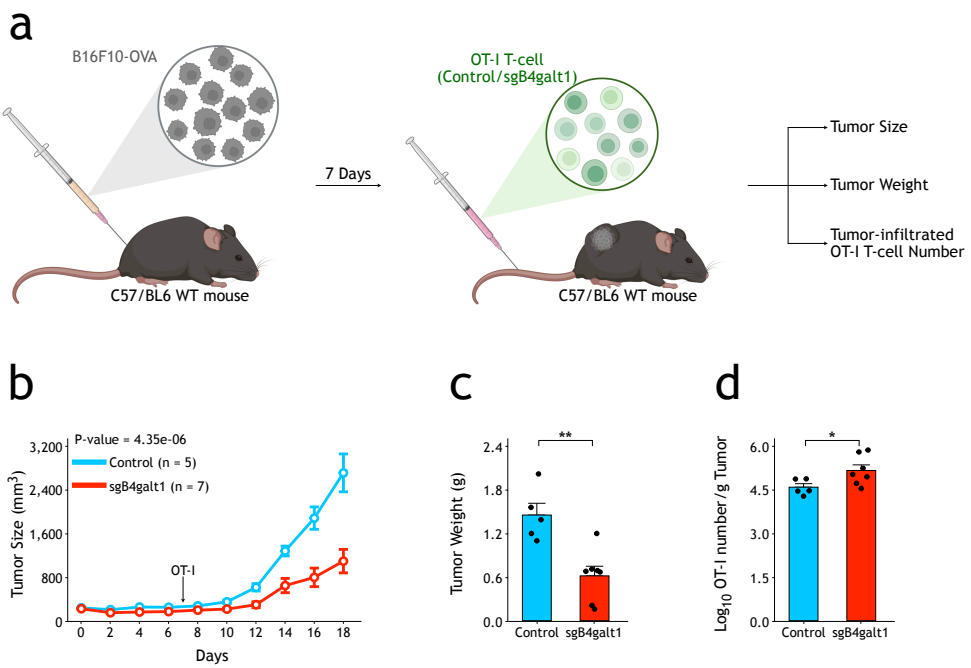
a
B16F10-OVA
C57/BL6 WT mouse
7 Days
OT-I T-cell
(Control/sgB4galt1)
C57/BL6 WT mouse
Tumor Size
Tumor Weight
Tumor-infiltrated
OT-I T-cell Number
b
P-value = 4.35e-06
Control (n = 5)
sgB4galt1 (n = 7)
Tumor Size (mm3)
OT-I
Days
c
Tumor Weight (g)
Control
sgB4galt1
d
Log10 OT-I number/g Tumor
Control
sgB4galt1

Figure 4

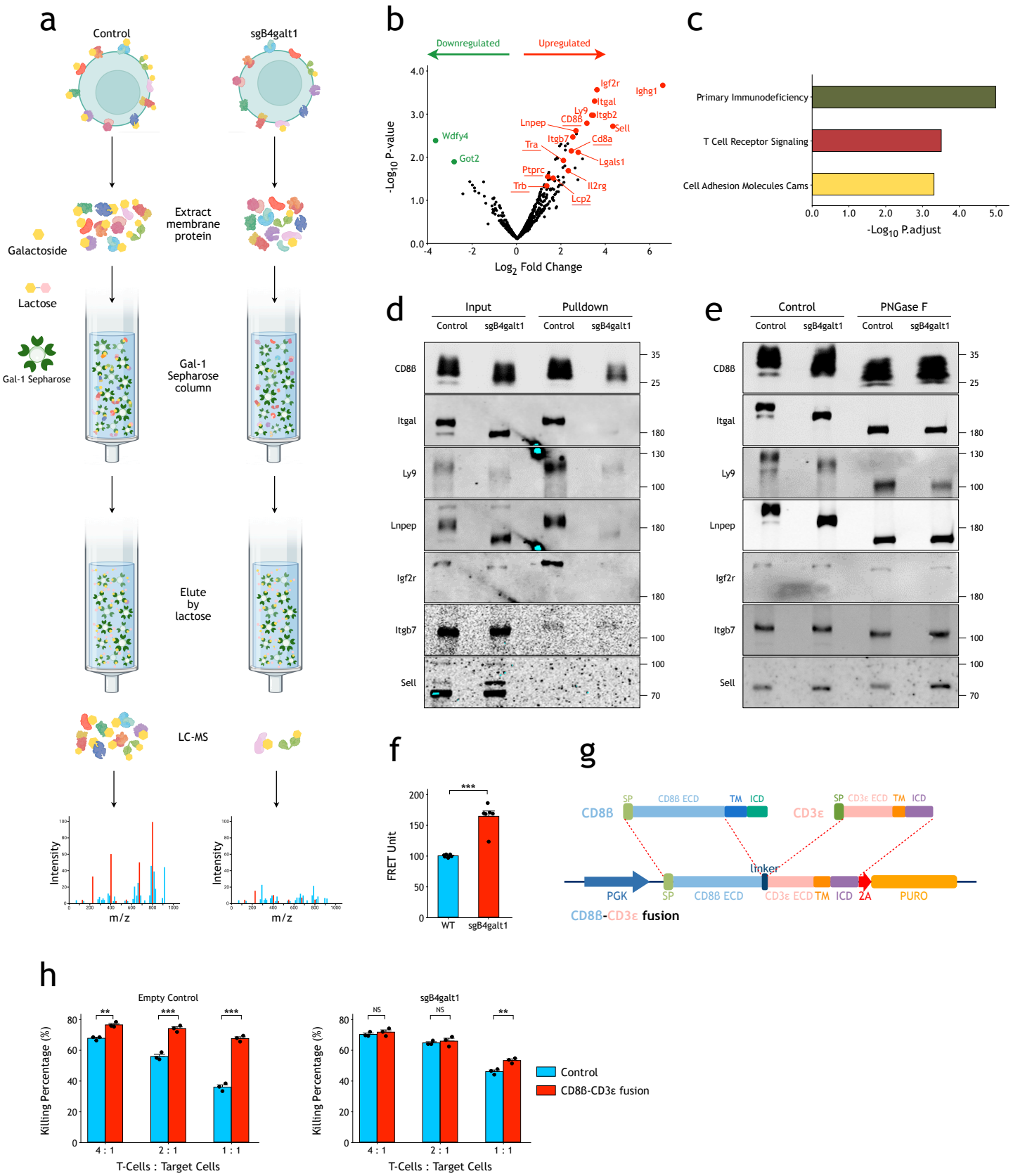
a
Control
sgB4galt1
Extract membrane protein
Galactoside
Lactose
Gal-1 Sepharose
Gal-1 Sepharose column
Elute by lactose
LC-MS
Intensity
m/z
b
Downregulated
Upregulated
-Log10 P-value
Log2 Fold Change
Igf2r
Ighg1
Itgal
Ly9
Itgb2
CD8B
Sell
Lnpep
Cd8a
Wdfy4
Itgb7
Tra
Lgals1
Got2
Ptprc
Il2rg
Trb
Lcp2
c
Primary Immunodeficiency
T Cell Receptor Signaling
Cell Adhesion Molecules Cams
-Log10 P.adjust
d
Input
Pulldown
Control
sgB4galt1
CD8B
Itgal
Ly9
Lnpep
Igf2r
Itgb7
Sell
e
Control
PNGase F
f
FRET Unit
WT
sgB4galt1
g
CD8B
SP
CD8B ECD
TM
ICD
CD3ε
CD3ε ECD
linker
PGK
2A
PURO
CD8B-CD3ε fusion
h
Empty Control
sgB4galt1
Killing Percentage (%)
T-Cells : Target Cells
4 : 1
2 : 1
1 : 1
NS
Control
CD8B-CD3ε fusion

Figure 5

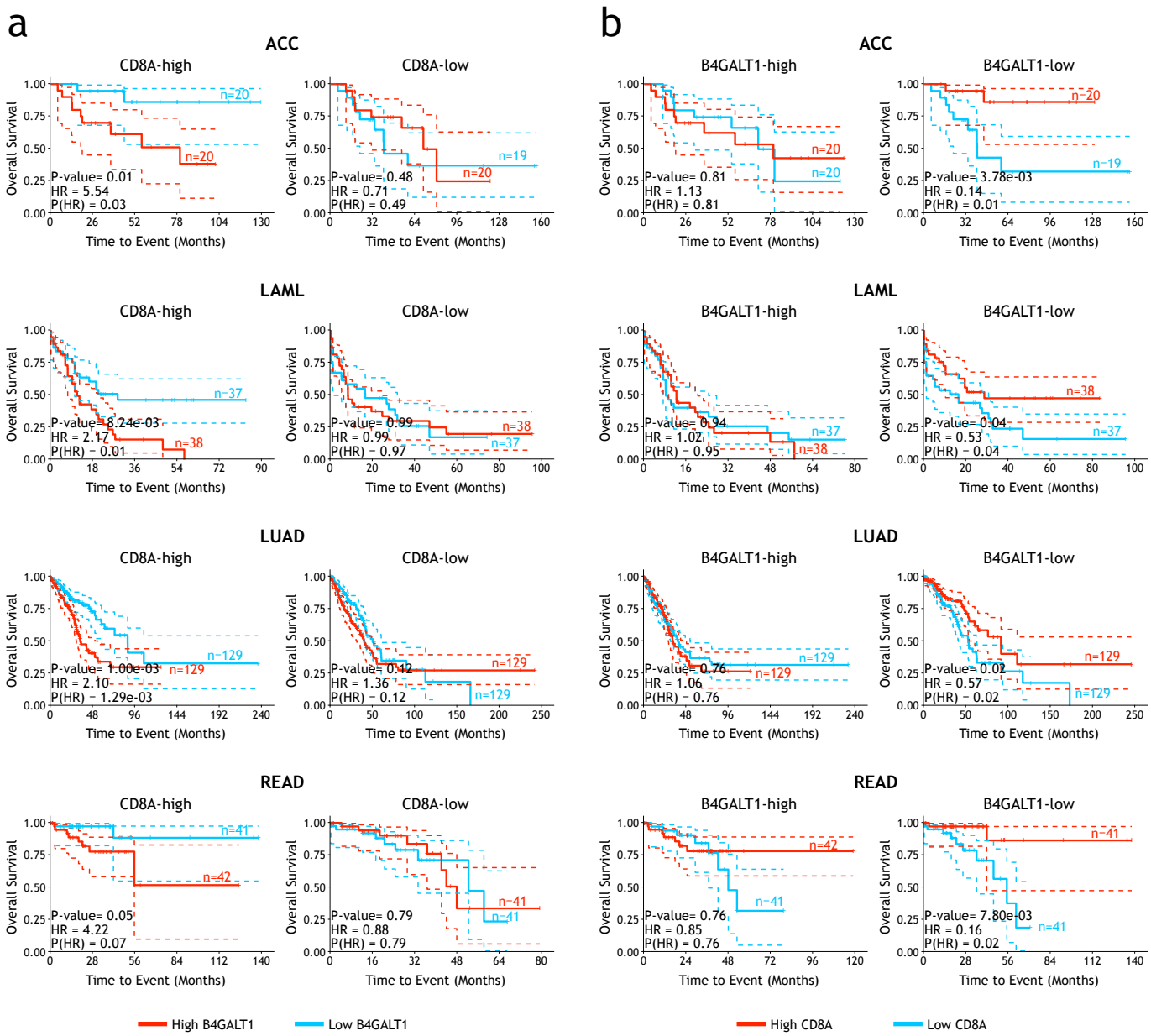
a
ACC
CD8A-high
P-value= 0.01
HR = 5.54
P(HR) = 0.03
n=20
n=20
CD8A-low
P-value= 0.48
HR = 0.71
P(HR) = 0.49
n=19
n=20
LAML
CD8A-high
P-value= 8.24e-03
HR = 2.17
P(HR) = 0.01
n=37
n=38
CD8A-low
P-value= 0.99
HR = 0.99
P(HR) = 0.97
n=38
n=37
LUAD
CD8A-high
P-value= 1.00e-03
HR = 2.10
P(HR) = 1.29e-03
n=129
n=129
CD8A-low
P-value= 0.12
HR = 1.36
P(HR) = 0.12
n=129
n=129
READ
CD8A-high
P-value= 0.05
HR = 4.22
P(HR) = 0.07
n=41
n=42
CD8A-low
P-value= 0.79
HR = 0.88
P(HR) = 0.79
n=41
n=41
High B4GALT1
Low B4GALT1
b
ACC
B4GALT1-high
P-value= 0.81
HR = 1.13
P(HR) = 0.81
n=20
n=20
B4GALT1-low
P-value= 3.78e-03
HR = 0.14
P(HR) = 0.01
n=20
n=19
LAML
B4GALT1-high
P-value= 0.94
HR = 1.02
P(HR) = 0.95
n=37
n=38
B4GALT1-low
P-value= 0.04
HR = 0.53
P(HR) = 0.04
n=38
n=37
LUAD
B4GALT1-high
P-value= 0.76
HR = 1.06
P(HR) = 0.76
n=129
n=129
B4GALT1-low
P-value= 0.02
HR = 0.57
P(HR) = 0.02
n=129
n=129
READ
B4GALT1-high
P-value= 0.76
HR = 0.85
P(HR) = 0.76
n=42
n=41
B4GALT1-low
P-value= 7.80e-03
HR = 0.16
P(HR) = 0.02
n=41
n=41
High CD8A
Low CD8A
Overall Survival
Time to Event (Months)

Figure 6